Summer 7-27-2021

Developing a Database of Seismic Data Over the Cascadia Subduction Zone

Khawlh Al Farsi
University of Nebraska-Lincoln, kalfarsi2@huskers.unl.edu

Developing a Database of Seismic Data Over the Cascadia Subduction Zone

An Undergraduate Senior Thesis
Bachelor of Science Degree in Geology
University of Nebraska-Lincoln

By
Khawlh Al Farsi,
BS Geology
College of Arts and Sciences

June 04, 2021

Faculty Mentor:
Irina Filina, Ph.D., Geophysics

Table of Contents

Abstract

An inevitable megathrust earthquake is expected in the Cascadia subduction zone that will affect the population of the coast of southwestern British Columbia and the northwest of the United States. In this active tectonic margin, the Juan de Fuca oceanic plate is subducting beneath the North American continental plate, causing unevenly distributed seismic activity. The major goal of this geophysical research project is to study the tectonic structures of the Cascadia subduction zone in order to comprehend the geology of the region and investigate the seismic hazards.

The primary objective of this project is to develop a geophysical database of published seismic refraction and reflection surveys over the Juan de Fuca plate and the Cascadia subduction zone. The resultant seismic reflection database consists of eight publicly available surveys that were acquired between 1964 and 2017. The total length of seismic reflection data covered by this project is ~13,250 km. Interpreting tectonic features over the Cascadia subduction zone using seismic reflections was challenged by the poor quality of vintage seismic images and by the lack of both vertical and horizontal scale markers. Despite that, seismic reflections allowed to interpret some shallow subsurface structures, although most of the old images did not map the depth to the Moho boundary.

Two publicly available seismic refraction surveys were also included in the database. These refractions surveys consist of two transects onshore and offshore in the states of Washington and Oregon, resulting in two-dimensional seismic velocity cross-sections. Compared to reflections, seismic refractions allowed for the interpretation of several deeper and larger tectonic structures, including the Moho boundary both in the continental and in the oceanic domains.

The second objective of this project focuses on developing an integrated two-dimensional geophysical model that utilized the thickness of various tectonic elements derived from seismic refraction and reflection data to model the free-air gravity anomaly. The model is 640 km long ranging from the Juan de Fuca spreading center on the west to onshore northern Oregon on the east. The model allowed to summarize the tectonic features of the entire study area, including several low-density zones in the oceanic subducting slab that were required in order to fit the observed free-air gravity anomaly.

Investigating crustal features and the structural architecture of the Cascadia subduction zone and the Juan de Fuca tectonic plate is important to comprehend the overall subduction process and understand the differences in the seismic activity along this active tectonic margin.

Introduction

The Cascadia subduction zone has been a region of multiple geological investigations and geophysical exploration over the past several decades (e.g., Morton et al.,1987; Trehu et al.,1994; Parsons et al.,1998; Han et al., 2016). It extends along the northwestern boundary of the North American continent (**Figure 1**) where the oceanic Juan de Fuca plate is subducting beneath the North American lithosphere at a rate of ~40 mm per year (DeMets et al., 1990).

Subduction zones occur where two tectonic plates collide with each other. Typically, a denser one of the two colliding tectonic plates (the oceanic one) is pulled beneath the other one into the Earth's mantle. The most devastating geological hazards, such as deep megathrust earthquakes and volcanic eruptions along with associated tsunamis and landslides, are typical for these active tectonic boundaries.

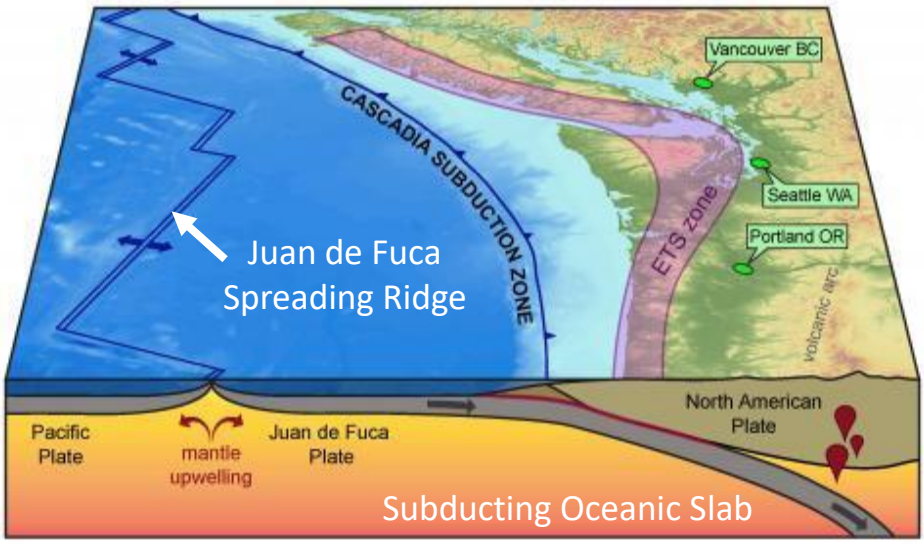

Figure 1. Cross-section of the Cascadia subduction zone from the United States Geological Survey. ETS stands for episodic tremor and slip events associated with subduction process. The red symbols above the subducting slab refers to volcanism.

According to the records by the United States Geologic Survey (USGS), the great earthquakes (with magnitudes ≥ 8.0) occurred in the geologic past in the Cascadia subduction zone. The recurrency interval period of megathrust earthquakes in this region is ~500 years (Atwater and Hemphill-haley, 1996; Witter et al., 2012; Goldfinger et al., 2017). However, earthquakes of

smaller magnitudes are typical for the study area, although they are not distributed evenly along the western coast of the United States (**Figure 2**) with noticeably fewer earthquakes in Oregon than in other regions of the Cascadia subduction zone.

According to Lillie (1999), an earthquake is a sudden release of stored within the Earth energy due to the failure of rocks to handle the exerted stresses. As the rocks rebound to a new position, seismic waves are generated. Relatively low seismic activity in a particular region of the Cascadia subduction zone indicates that the strain energy is being stored in the subsurface and will be released in the form of a powerful and devastating earthquake in the future.

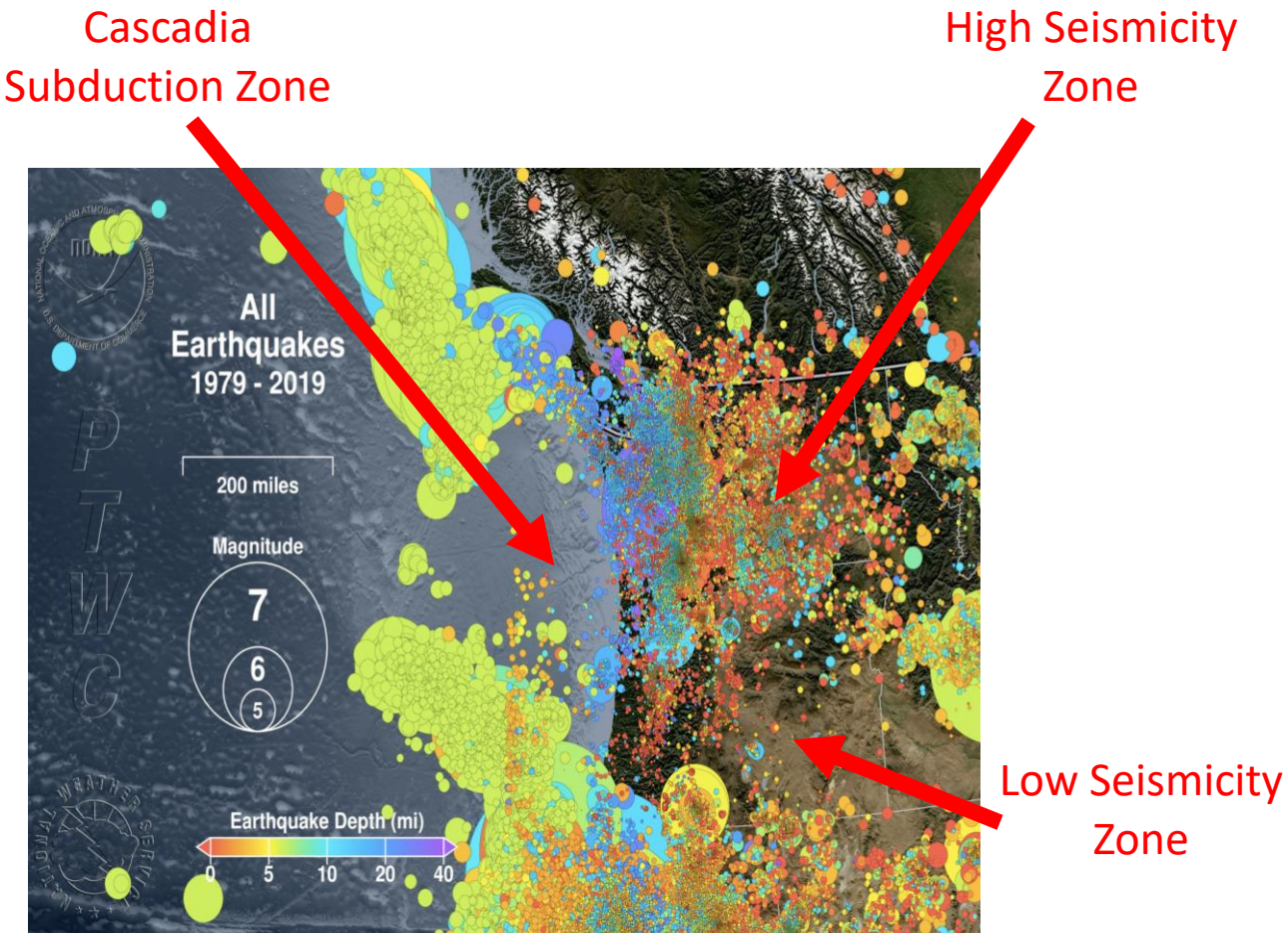

Figure 2. Recorded seismic activity along the Cascadia subduction zone between 1997 and 2019. The size and color of each circle indicate the magnitude and depth of the recorded earthquake. Screenshot from the video "Earthquakes of Cascadia: 1979 – 2019." produced by the Pacific Tsunami Warning Center (2019).

This study has two main objectives. The first one is to compose a geophysical database of published seismic reflection and refraction surveys over the subducting Juan de Fuca oceanic plate and the Cascadia subduction zone. The second objective of this project is to develop a two-dimensional geophysical model of the area utilizing the seismic reflection and refraction database and free-air gravity readings to summarize the overall geological architecture and tectonic structures associated with the ongoing subducting process.

The differences and similarities between seismic reflection and refraction methods are summarized in Chapter 1. Chapters 2 and 3 are focused on the first objective of this project - Chapter 2 describes the main findings of the developed reflection database, whereas Chapter 3 outlines the key seismic refraction surveys. The fourth chapter targets the second objective and describes an integrated two-dimensional model that was developed based on the seismic data and a measured free-air gravity anomaly.

Chapter 1. Seismic Reflection and Refraction Experiments

Seismic reflection and refraction are two distinct active geophysical methods that are used for geophysical exploration of both shallow and deep subsurface structures. Both methods require a source that generates seismic sound waves. Examples of seismic sources that can be used for onshore investigations are hammers, explosives, or a seismic vibrating machine that is known as a Vibroseis. In offshore settings, the explosive sources, such as dynamites, that used to be common in the last century, are now replaced by air guns as they are more friendly for marine life.

Figure 3 shows a typical seismic survey in offshore settings. A hydrophone is an offshore instrument that records seismic waves after the acoustic energy gets reflected or refracted through the subsurface. Onshore, geophones are used as receivers of seismic energy that record ground motion in different directions. The recorded seismic trace is used to derive geological parameters, such as the depth to subsurface geological structures and velocities of seismic waves in individual layers.

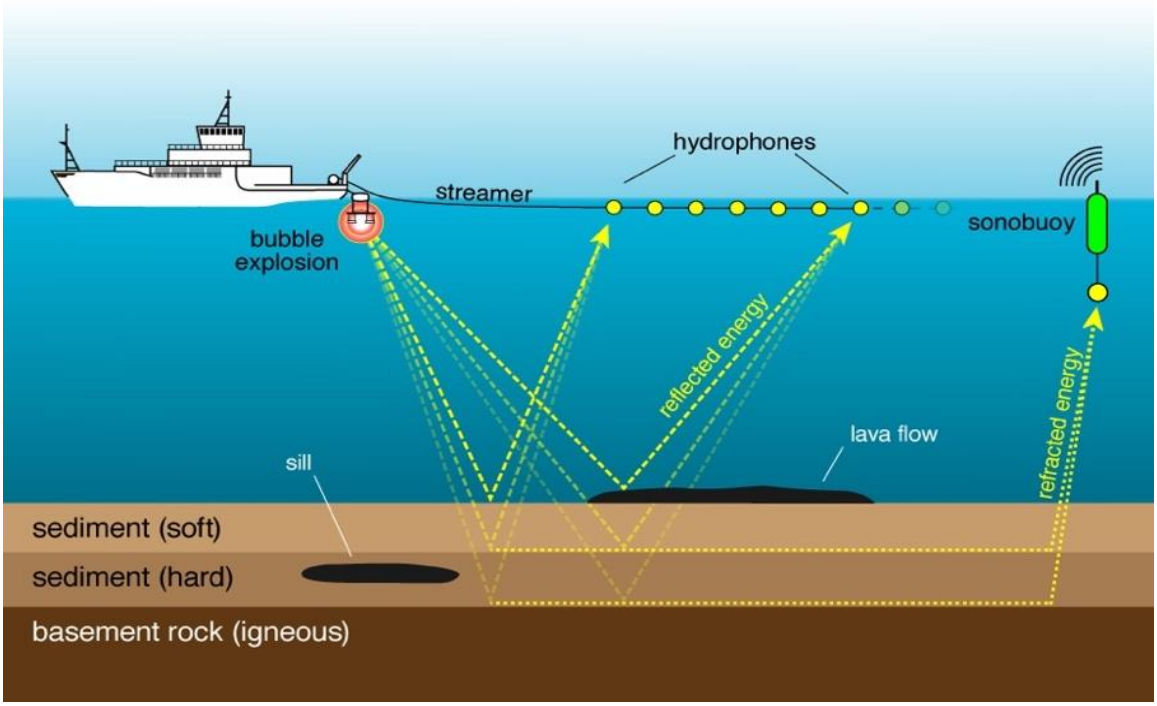

Figure 3. An offshore seismic experiment illustrating both reflection and refraction seismic ray paths. Image from CoastalReview.org.

Although both seismic reflection and refraction methods measure either ground motion (onshore) or water pressure (offshore, as is shown in **Figure 3**), the derived parameter differs depending on each method. A typical reflection experiment images subsurface geological structures, while refraction derives the velocities of seismic waves in the subsurface rocks.

The seismic reflection method relies on the fact that the subsurface of the Earth consists of different rock layers. As the incident seismic wave travels from the source through the first rock layer (**Figure 4a**), it hits the interface with the second layer with a different acoustic impedance and accordingly reflects back to the receivers. The amount of reflected energy depends on the difference in acoustic impedance of the rock layer forming the interface. Acoustic impedance is the product of density and the compressional seismic velocity of a rock layer. The rest of the energy refracts - propagates at a different angle to the next rock layer. The angle of refraction may be computed using Snell's law:

$$\frac{\sin \theta 1}{V\,1} = \frac{\sin \theta 2}{V\,2}$$

where:

$\theta 1$ = angle of incidence
$\theta 2$ = angle of refraction
V1 = seismic velocity of the incident medium
V 2 = seismic velocity of the refracting medium.

Figure 4b shows the propagation of seismic energy for the system with multiple rock layers.

a. b.

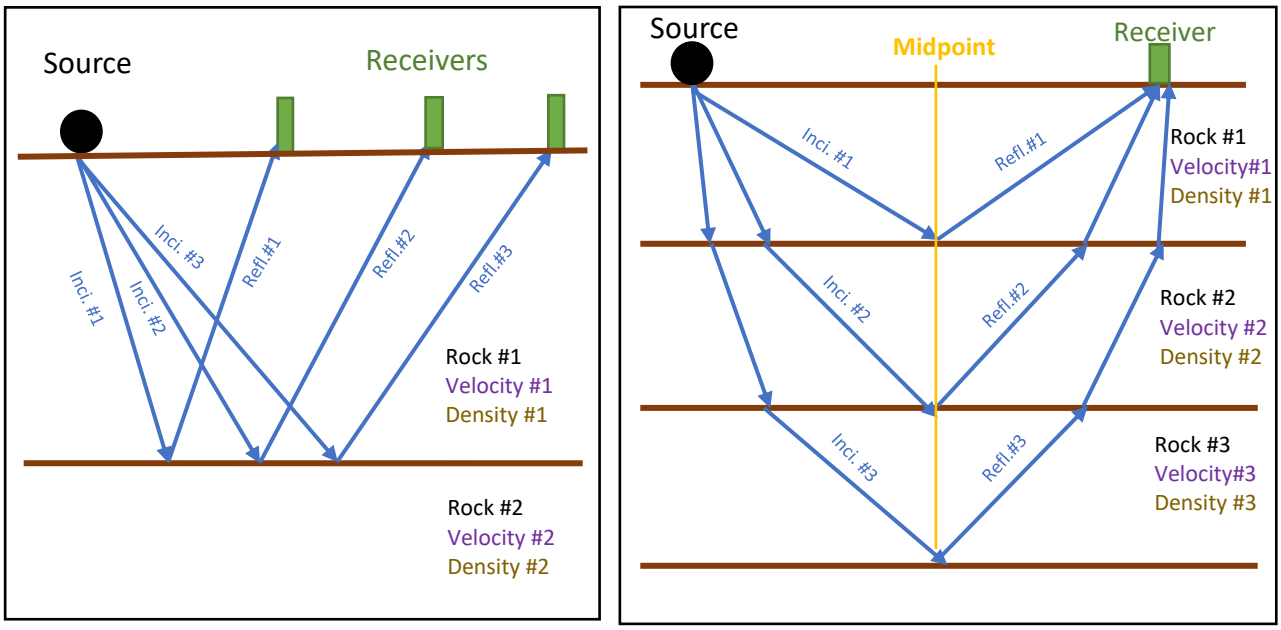

Figure 4. a. Seismic reflections in a two-layers model. **b.** The propagation of seismic energy through a multiple-layers model.

In contrast, the seismic refraction method derives the velocity of seismic waves propagation through the subsurface layers, which serve as proxies to lithologies. Critical refraction, as shown in **Figure 5a**, occurs when the angle between the incident ray and the vertical leads to refraction at a right angle (90°), forcing the seismic energy to propagate along the interface between two layers of rocks. The compressional velocity must increase with depth for critical refraction to occur, as is shown in **Figure 5b**.

Figure 6 shows the travel-time plot that includes several seismic arrivals from a single source to a spread of receivers. It includes a direct ray (**Figure 5a**), reflected ray (**Figure 4a**; it appears as a hyperbola), and refracted ray (**Figure 5a**; a straight line). A comparison between seismic reflection and refraction techniques is summarized in **Table 1**.

a. b.

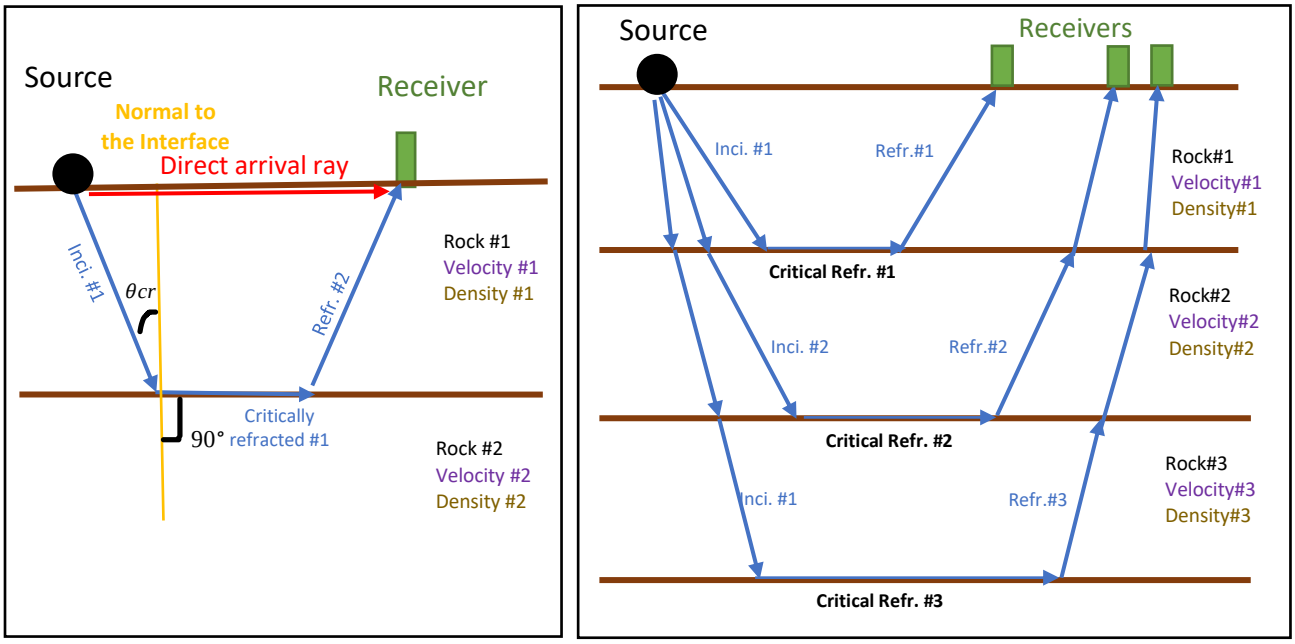

Figure 5. a. Critical refraction in a two-layers model. **b.** Multiple-layers model with critical refractions to multiple receivers from a single source.

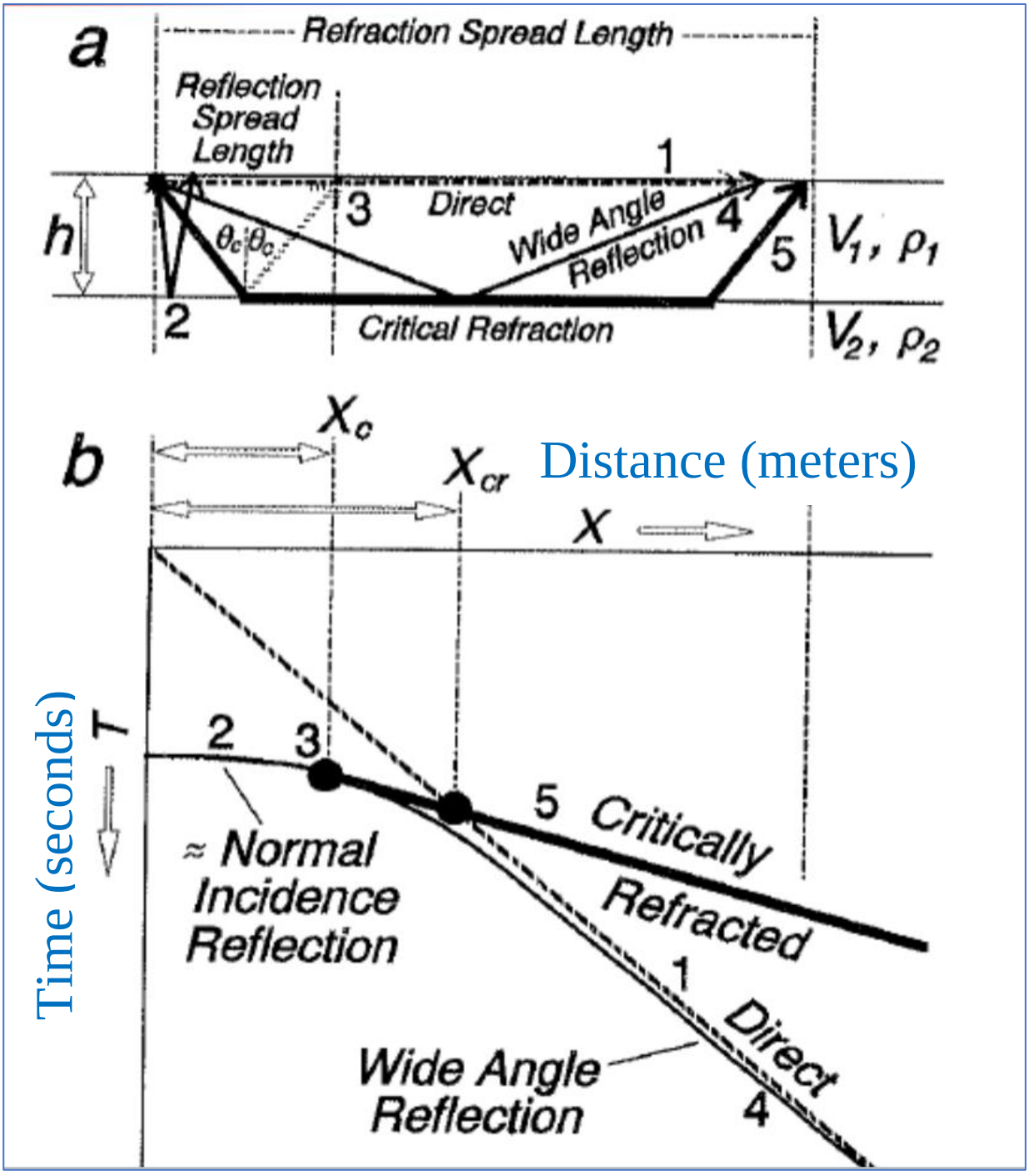

Figure 6. Distance-time plot of direct, reflected, and refracted arrivals. X_{cr} is crossover distance, and X_c is critical distance. Image from Lillie (1999).

Table 1. Comparison between seismic reflection and refraction techniques.

	Reflections	**Refractions**
Measured parameter	Ground Motion (Onshore)/Water Pressure (Offshore)	Ground Motion (Onshore)/Water Pressure (Offshore)
Derived information	Subsurface structures	Velocities
Seismic record on travel-time plot	Hyperbola	Straight line

Chapter 2. Seismic Reflection Surveys

The subducting Juan de Fuca oceanic plate has different tectonic structures, such as spreading centers, transform faults, propagator wakes and seamounts. Seismic methods are traditionally used to map those structures. The locations of seismic reflection and refraction records covered by this project are shown in **Figure 7**.

This project accounts for a series of eight published seismic reflection surveys over the Juan de Fuca plate. These surveys were conducted over more than fifty years between 1964 and 2017. **Table 2** lists the found reflection surveys ordered by their published year from oldest to youngest.

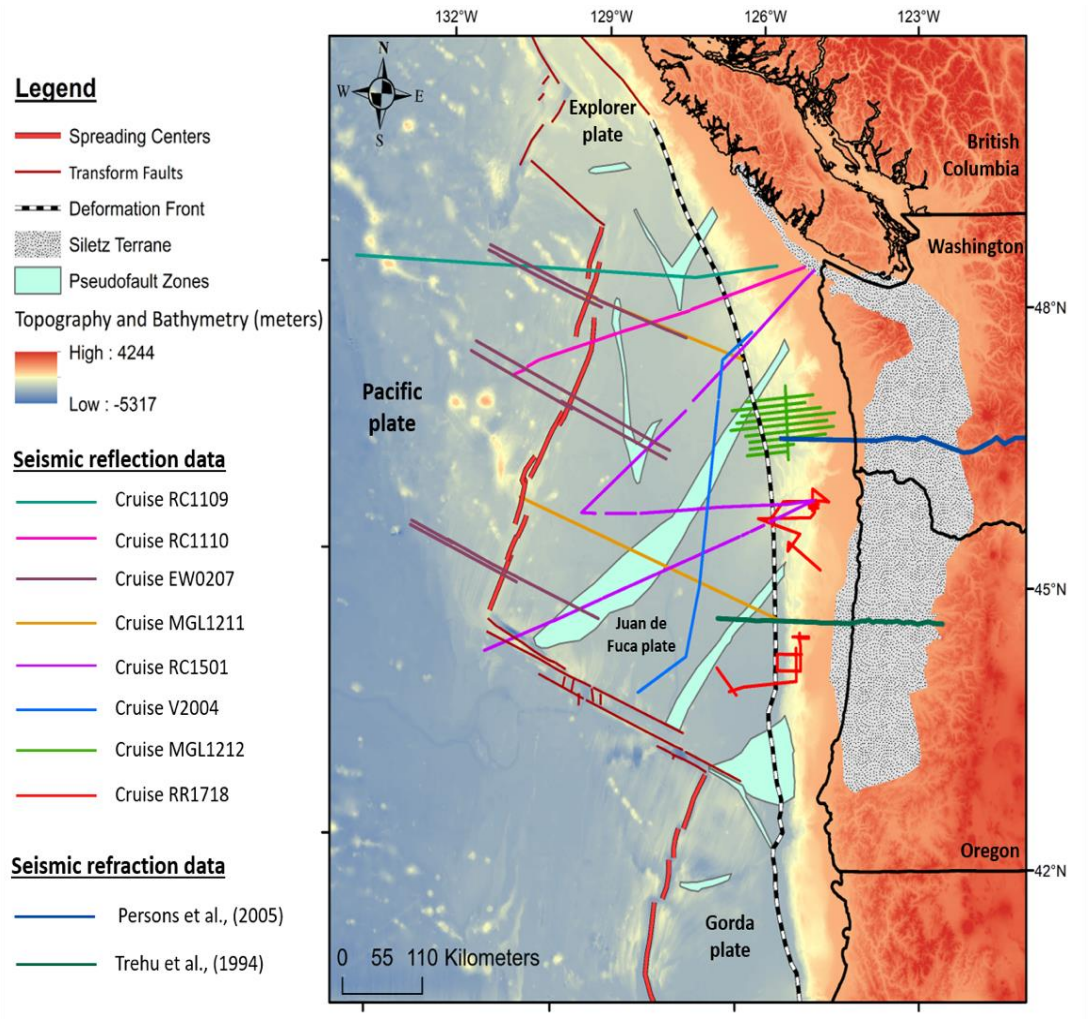

Figure 7. Published seismic reflection and refraction surveys over the Juan de Fuca plate (map was prepared by Asif Ashraf, 2021)

Table 2. Summary of seismic reflection surveys covered by this project.

Survey Name	Year	Total length (km)	Reference
V2004	1964	486	Le Pichon, X.1964, V2004
RC1109	1967	581	Pitman, W. 1067, RC1109
RC1110	1967	255	Epp, D. ,1967, RC1110
RC1501	1971	1239	Carpenter, G. ,1971, RC1501
EW0207	2002	8160	Canales, J. , 2002, EW0207
MGL1211	2012	576	Carbotte, S. , Canales, J. , 2012, MGL1211
MGL1212	2012	855	Holbrook, S., 2012, MGL1212,
RR1718	2017	1101	Tominaga, M. 2017, RR1718

2.1 Methodology

Seismic images, such as the ones shown in **Figure 8a**, were downloaded from public sources (see references listed in **Table 2**). The majority of seismic images are old, unscaled, and of poor quality. The RC1501 seismic reflection survey (Carpenter, 1971) serves as a good example to illustrate a stitching method that was applied to fix these images, scale them properly, and ultimately arrange them into a coherent seismic profile. This survey was conducted in 1967 and the results are available in form of twelve individual seismic images.

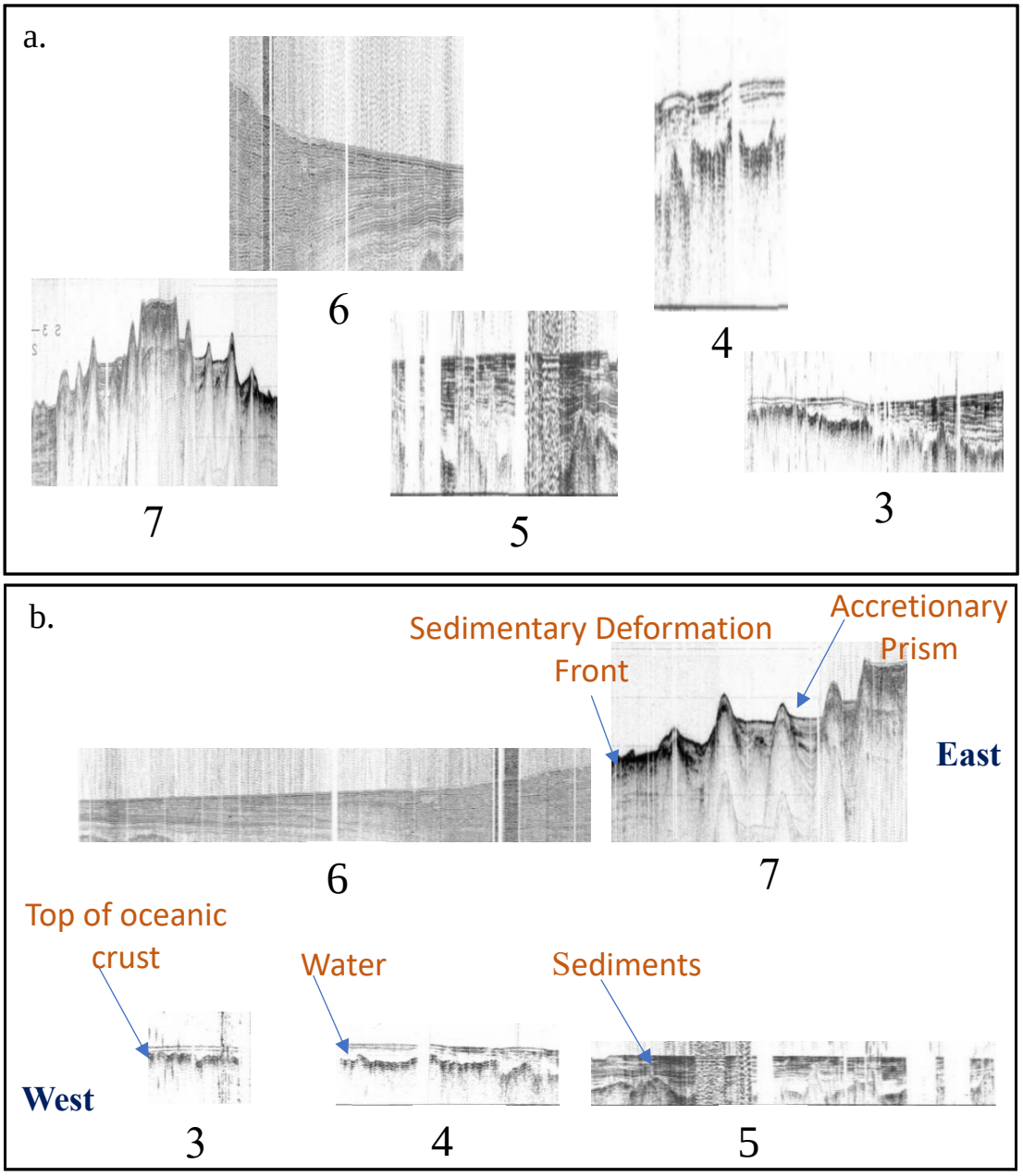

Figure 8. a. Original seismic images as found in the published RC1501 reflection data (Carpenter, 1971). **b.** Stitched seismic reflection profile of the RC1501 survey.

A screenshot of the published map of the RC1501 reflection survey over the Juan de Fuca plate is shown in **Figure 9a**, while **Figure 9b** shows the graph of the waypoints downloaded along with the images of the RC1501 survey. The initial geographic coordinates (latitude and longitude) of each waypoint were converted to Cartesian X and Y using the UTM10N projection. **Table 3** lists all the coordinates for the RC1501 survey.

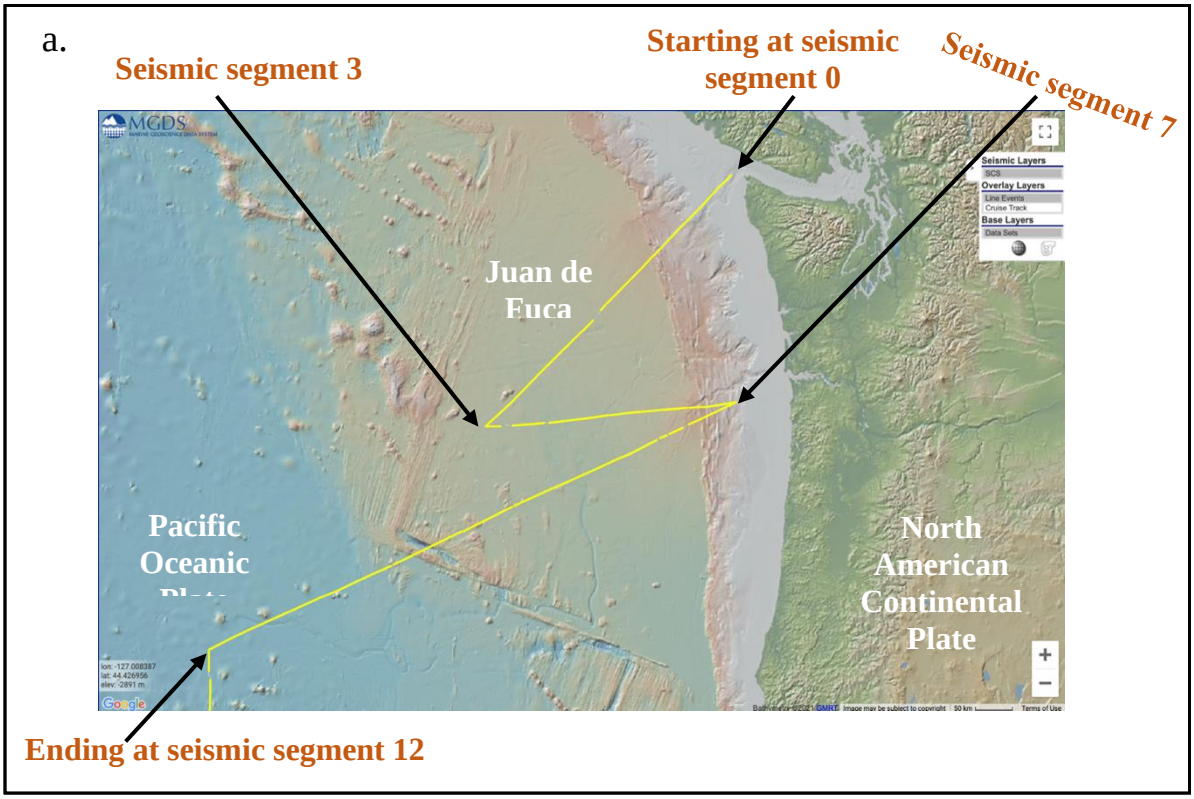

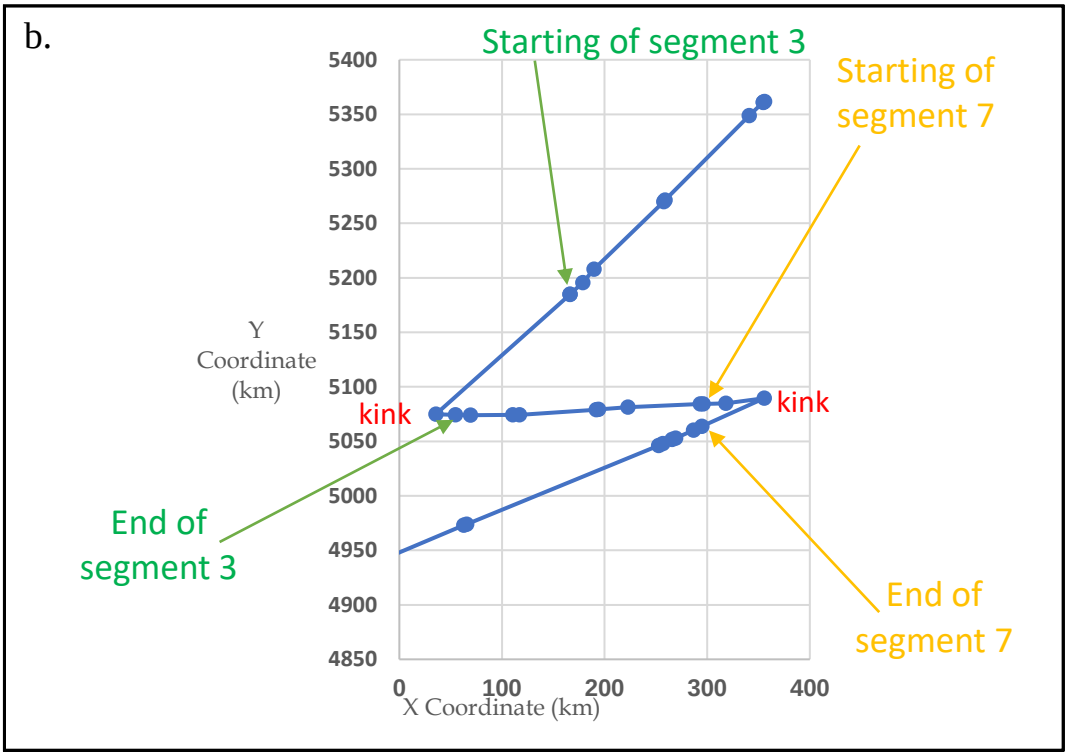

Figure 9. a. The location of the seismic reflection survey RC1501 over the Juan de Fuca plate (the screenshot from Marine Geoscience Data System). **b.** Graph of the waypoints of RC1501 reflection survey converted to Cartesian coordinates in UTM 10N.

Table 3. Seismic reflection waypoints and coordinates of RC1501 survey.

Seismic Segment Number	Longitude	Lattitude	X Coordinate, Long. 10N, km	Y Coordinate, Lat. 10N, km	**Length, km**	**Distance from start, km**
12	-130.47727	44.116631	-98.35866783	4912.085174	99	
12	-129.35959	44.49349	-5.647916356	4946.394068	2	
11	-129.3344	44.4974	-3.610514149	4946.672231	71	101
11	-128.5267	44.775399	62.70772535	4972.878463	3	
10	-128.4919	44.7866	65.54539653	4973.93569	200	175
10	-126.16808	45.524304	252.5965606	5046.079686	4	
9	-126.1166	45.541902	256.6925828	5047.877253	10	380
9	-126.004	45.5776	265.6318141	5051.507685	4	
8	-125.9601	45.5915	269.1137357	5052.924493	19	394
8	-125.73849	45.661397	286.664429	5060.075263	9	
7	-125.63529	45.695091	294.8274281	5063.548742	66	421
7	-124.8662	45.9437	355.3500539	5089.485459	37	
7	-125.34365	45.89344	318.1789089	5084.878957	22	
7	-125.6293	45.881099	295.9739898	5084.198818	3	
6	-125.66674	45.879416	293.0625606	5084.108294	70	428
6	-126.5691	45.829457	222.793503	5081.296115	29	
6	-126.9368	45.798701	194.0672661	5079.222883	2	
5	-126.9656	45.7962	191.8155581	5079.055847	75	335
5	-127.9231	45.7166	116.8630387	5074.358921	7	
4	-128.0073	45.7117	110.2765129	5074.222105	9	264
4	-128.5323	45.686	69.22050279	5074.064877	15	
3	-128.72	45.6783	54.54483253	5074.239651	19	223
3	-128.9639	45.6724	35.50348007	5074.974509	171	
3	-127.3708	46.7323	166.0707542	5184.699528	0	
2	-127.3674	46.7346	166.3446949	5184.940612	16	380
2	-127.2119	46.8343	178.8175852	5195.368824	16	
1	-127.0794	46.9511	189.5960918	5207.811868	92	413
1	-126.2209	47.5369	257.6041688	5269.859379	2	
0	-126.2047	47.5483	258.8755527	5271.075685	113	506
0	-125.14442	48.271178	340.8800001	5348.664016	18	
0	-124.96258	48.384994	354.6959467	5360.953023	0	
0	-124.9649	48.382258	354.516611	5360.653326	2	
0	-124.9497	48.391299	355.6674856	5361.629446		

Figure 8a shows five separate images (3 to 7) from the central segments of that survey, while **Figure 8b** shows the result of applying a stitching procedure to original published seismic reflection images of the RC1501 survey. For example, seismic images 3 and 7 were cropped and mirrored (compare **Figures 8a** and **8b**). The particular challenge was in determining both the horizontal and vertical scales for each image. The horizontal scale was computed from coordinates (**Table 3**) and later validated with bathymetry data (Smith and Sandwell, 1997). After all individual images were aligned, scaled, and stitched together, the resultant profile was ready for geological interpretation.

2.2 Seismic reflection database

Tectonic structures interpreted from seismic reflections over the Juan de Fuca plate and along the Cascadia subduction zone vary depending on the location. For instance, the top of the oceanic crust, sedimentary layers, accretionary wedge, and sedimentary deformation front can be interpreted from the RC1501 reflection images (**Figure 8b**, see location in **Figure 9b**). In addition, some other geological features can be observed in another portion of this survey, particularly in seismic segments 10 (northeast) through 12 (southwest) shown in **Figure 10**. The dark blue dotted line in **Figure 10** follows several exposed bathymetric seamounts, while smaller buried seamounts to the east can be interpreted from the basement overlain by sediments that is shown in red. Light

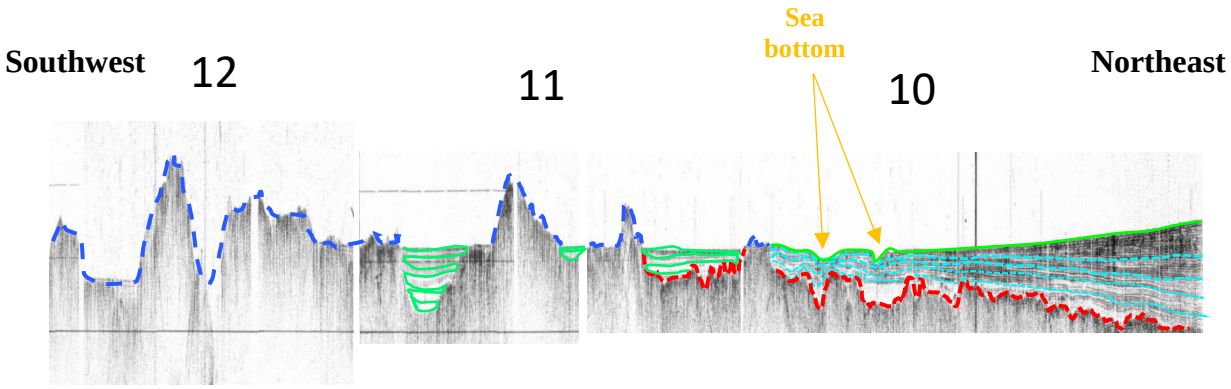

Figure 10. Stitched seismic reflection profile from images 10 to 12 of the RC1501 survey (Carpenter, 1971). Colored features are described in text.

green lines show sedimentary basins between the seamounts, while the horizontal sedimentary strata that thicken to the east are represented as light blue dotted lines.

In some seismic reflection surveys covered by this project, the stitching method was not the main challenge due to the fewer number of seismic images, such as the V2004 survey shown in **Figure 11**. Identifying the location of the kinks along the seismic line was the main problem instead. To tackle that, the bathymetric measurements from Smith and Sandwell (1997) were used to align with the seismic images and ultimately determine the locations of the turning points.

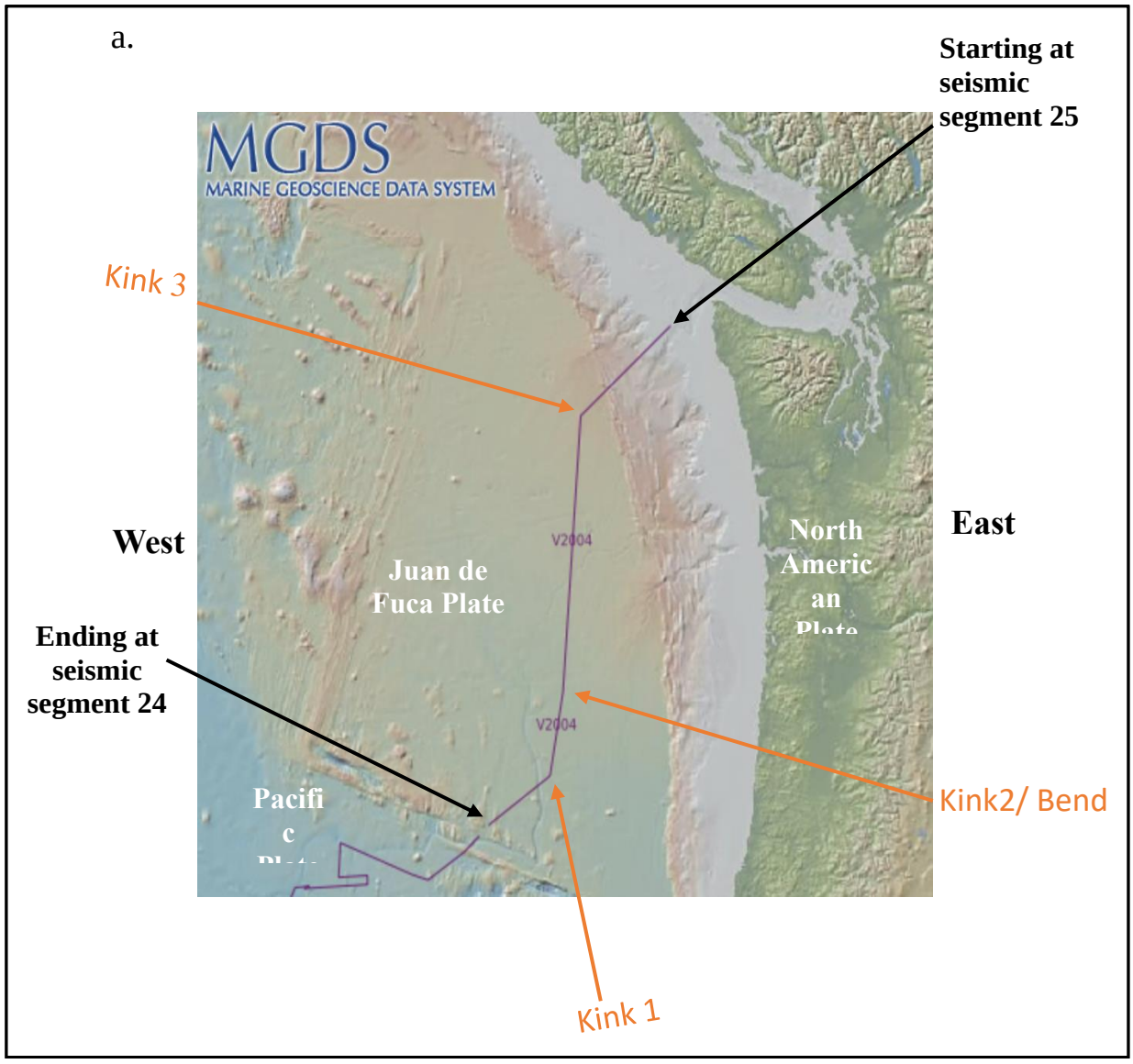

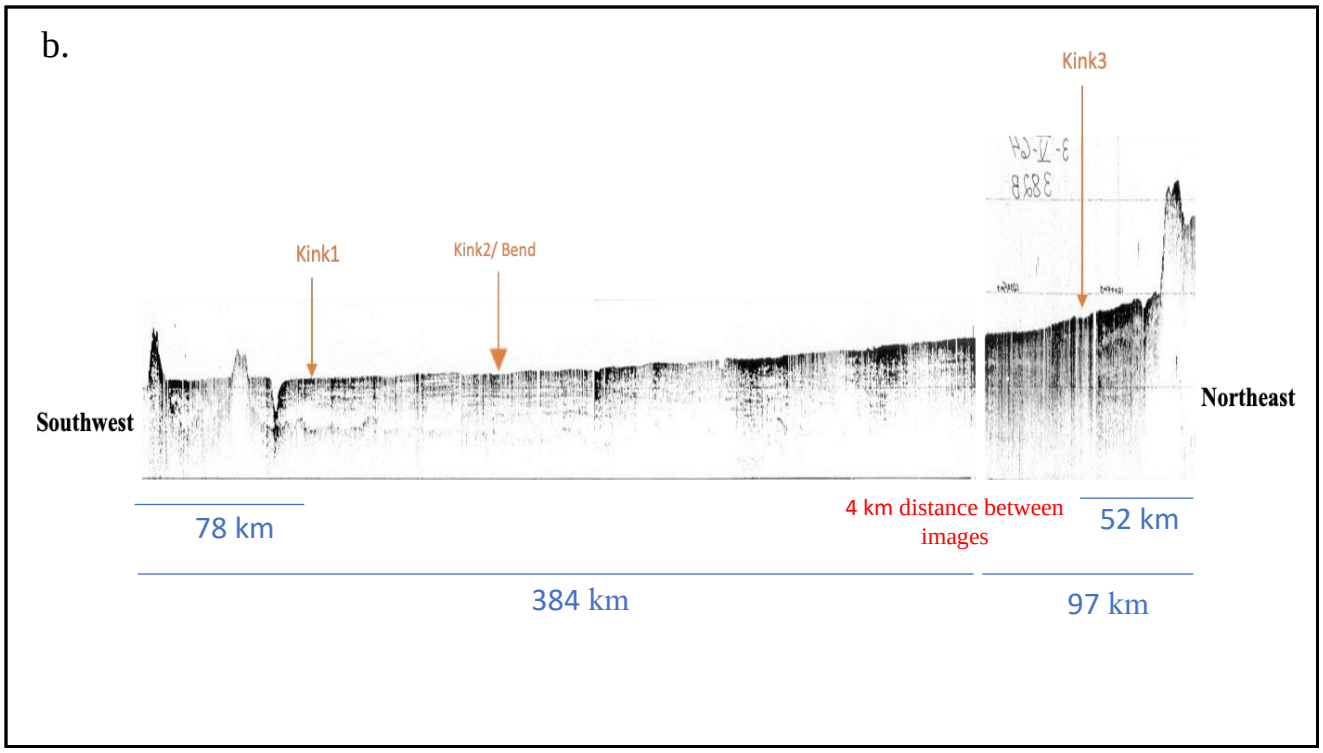

Figure 11. a. Location of the seismic reflection survey V2004 (Le Pichon,1964) over the Juan de Fuca plate. **b.** Identified kinks in the V2004 seismic reflection stitched profile.

Tectonic interpretations in other seismic reflection surveys were challenged by the noise in seismic images and faint reflections. For example, in the survey RR1718 (Tominaga, 2017; Line 5 is shown in **Figure 12**), the accretionary prism and individual folds are nicely imaged. However, the first multiple in the bottom of the seismic image masks the base of the accretionary prism and prevents the interpretation of deeper tectonic structures without reprocessing the real seismic record.

Some recent seismic reflection surveys provide clearer images that did not require any stitching. Particularly, the seismic reflection surveys EW0207 and MGL1211 (see locations in **Figure 7**) were acquired in 2002 and 2012, respectively. According to Han et al. (2016), a combination of these two surveys allowed to develop two seismic depth models across the Juan de Fuca oceanic plate in the Washington and Oregon sides of the margin shown in **Figure 13**.

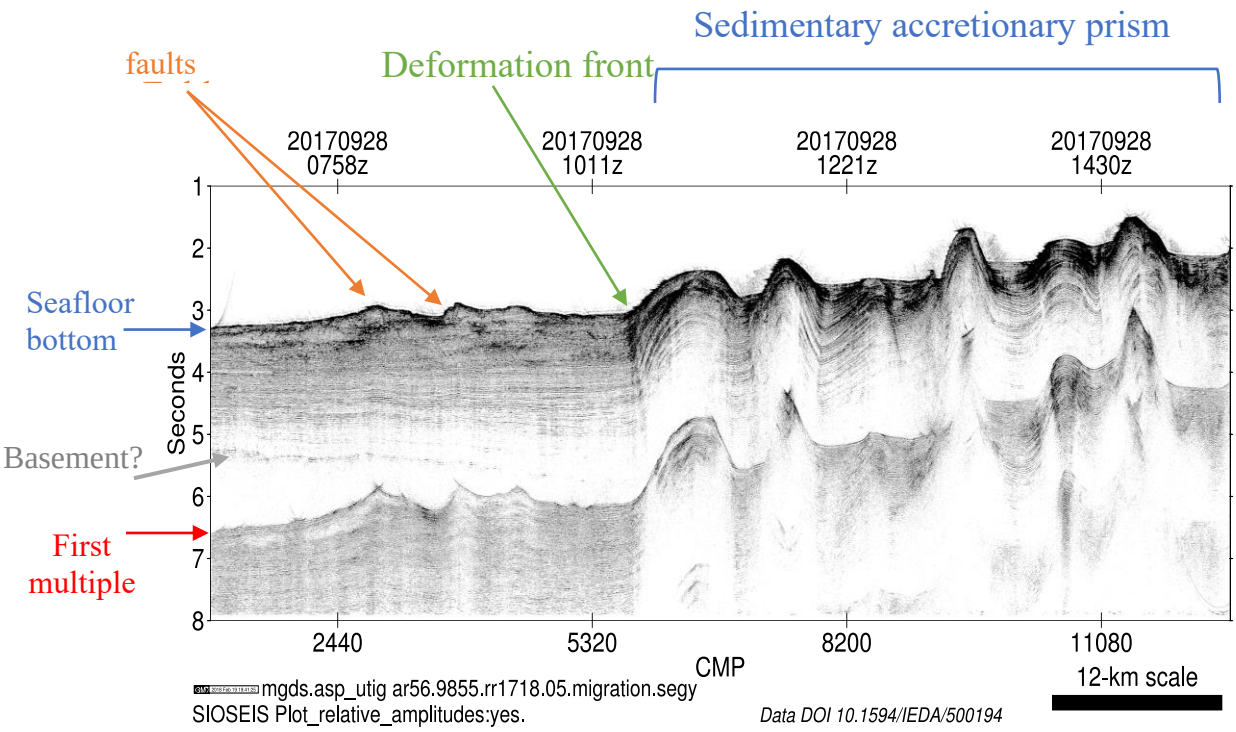

Figure 12. Example of seismic reflection line 05 from the RR1718 survey (Tominaga, 2017). Red arrow points to the first multiple of reflection data, that causes difficulties in interpretation.

Tectonic structures interpreted from these two sections include the top of the seafloor and the top and the bottom of the entire oceanic plate (the basement and Moho, respectively), allowing to measure the crustal thickness (~6.5 km), as well as to image multiple crustal and mantle faults.

The majority of seismic cross-sections in the developed database are a two-way travel time domain (i.e., they have seconds as a unit for a vertical axis). Only three surveys EW0207, MGL1211 and MGL1212 have data converted from time in seconds to depth in kilometers. In order to do that, the acoustic velocities of water, sediment, and the crust are required. However, as was described in Chapter 1, seismic reflection data do not allow to measure acoustic velocities, so seismic refraction experiments are required.

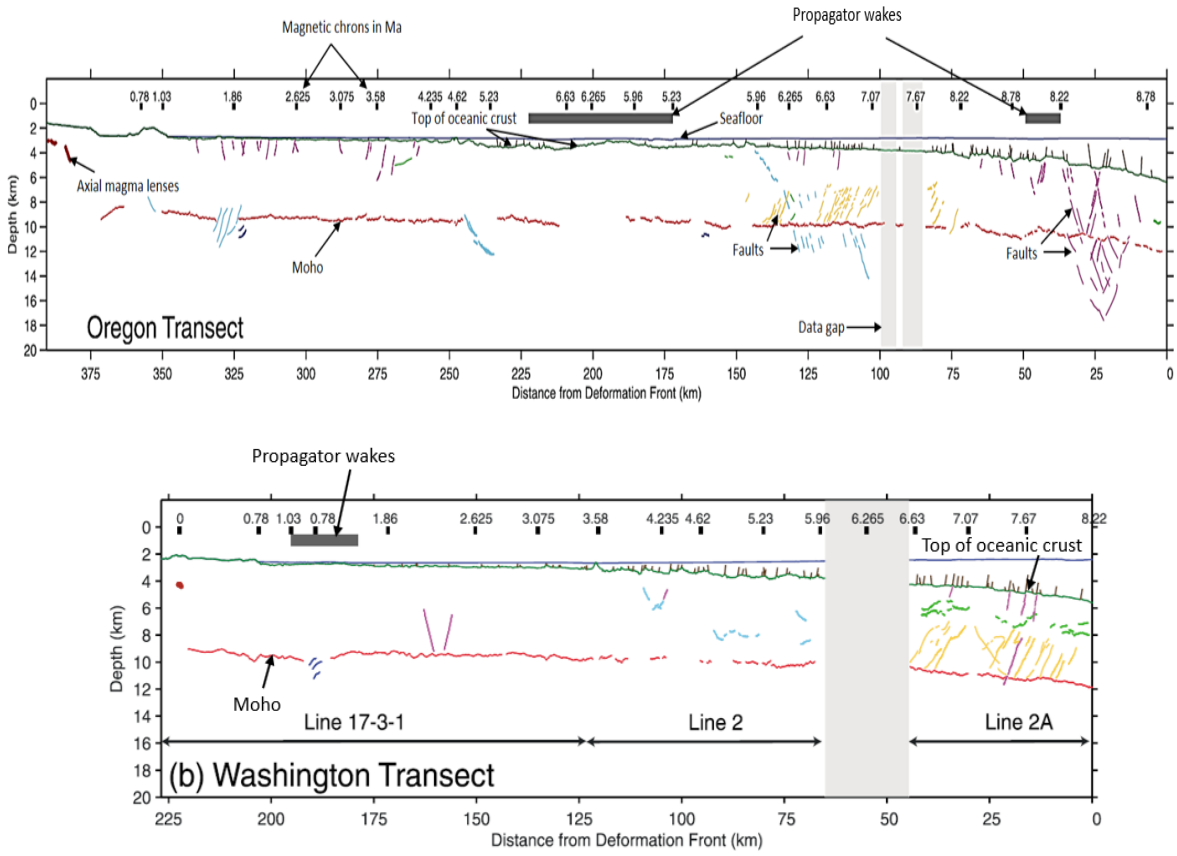

Figure 13. Cross sections from Oregon (a) and Washington (b) transects from Han et al., (2016). These lines combine surveys MGL1211 and EW0207 (see locations in **Figure 7**). Colored features are interpreted as follows; red is the Moho boundary, green is the top of the oceanic crust, blue is the seafloor, and the rest are crustal and mantle faults.

Chapter 3. Seismic Refraction records

As was mentioned in Chapter 1, seismic reflection data respond to contrasts in acoustic impedances of the contacting rock layers (the product of velocity and density), while seismic refractions depend on the contrast in seismic velocity only. A typical seismic refraction experiment requires the velocity of layered rocks to increase with depth in order to generate critically refracted seismic sound waves (see **Figure 5b**).

Two main seismic refraction experiments conducted across the northwestern coast of the United States are covered by this project. As shown in **Figure 7**, the first seismic refraction profile is located in the southwestern side of Washington state, whereas the second transect crosses the northwestern portion of Oregon state. **Table 4** summarizes these two seismic refraction surveys.

Table 4. Summary of siesmic refraction surveys coverd by this project.

General Location	Profile Number	Length of profile, km	Reference
Washington	1,2,3,4,5,6,10,11,12	520 km	Geomar, 1996
Oregon	7,8,9	300 km	Geomar, 1997

The southern Washington transect is described by Parsons et al. (2005). **Figure 14** shows the resultant two-dimensional velocity cross-section that enabled interpreting not only the subducting Juan de Fuca slab, but also several other tectonic features, such as the oceanic crust to the west of the deformation front, the sedimentary accretionary prism, the accreted Siletz terrane, and the Cascade arc. This cross-section also allowed to measure the thickness of each subsurface layer interpreted from changes in measured seismic velocity.

Trehu et al. (1994) interpreted the second seismic refraction line covered by this project. This line was collected at the same time as the line of Parsons et al. (2005), but in the Oregon part of the margin, as shown in **Figure 7**. The resultant two-dimensional velocity model is shown in

Figure 15. The main difference between the two refraction experiments is in an interpreted seamount pointed by a red arrow in **Figure 15**.

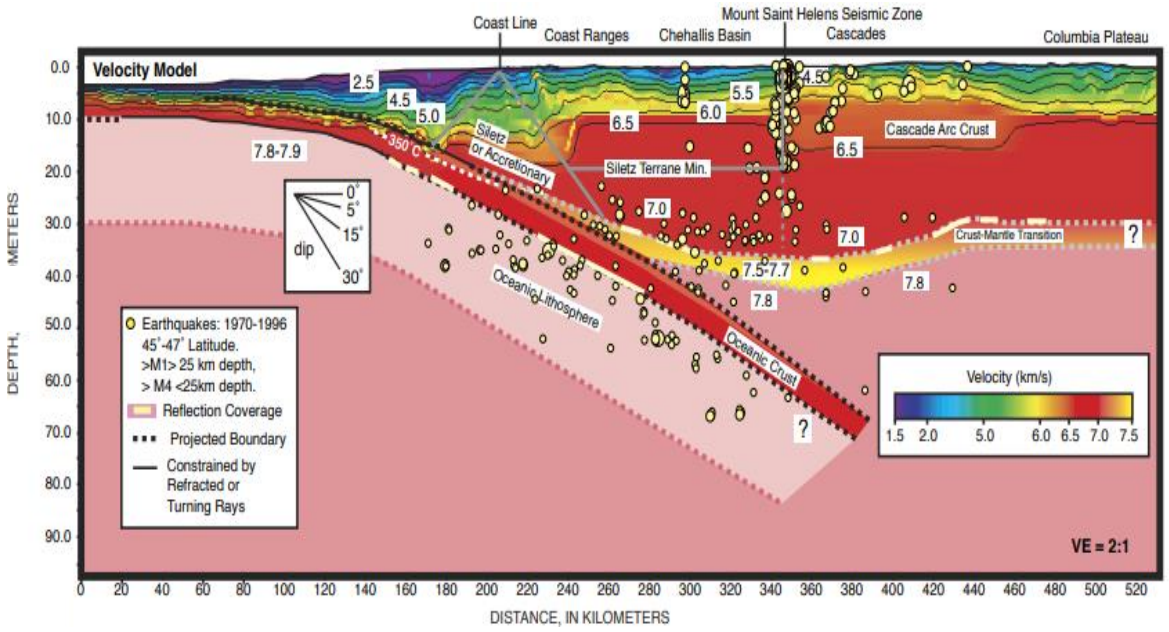

Figure 14. Two-dimensional velocity-structure model from refraction data across the Washington transect from Parsons et al. (2005)

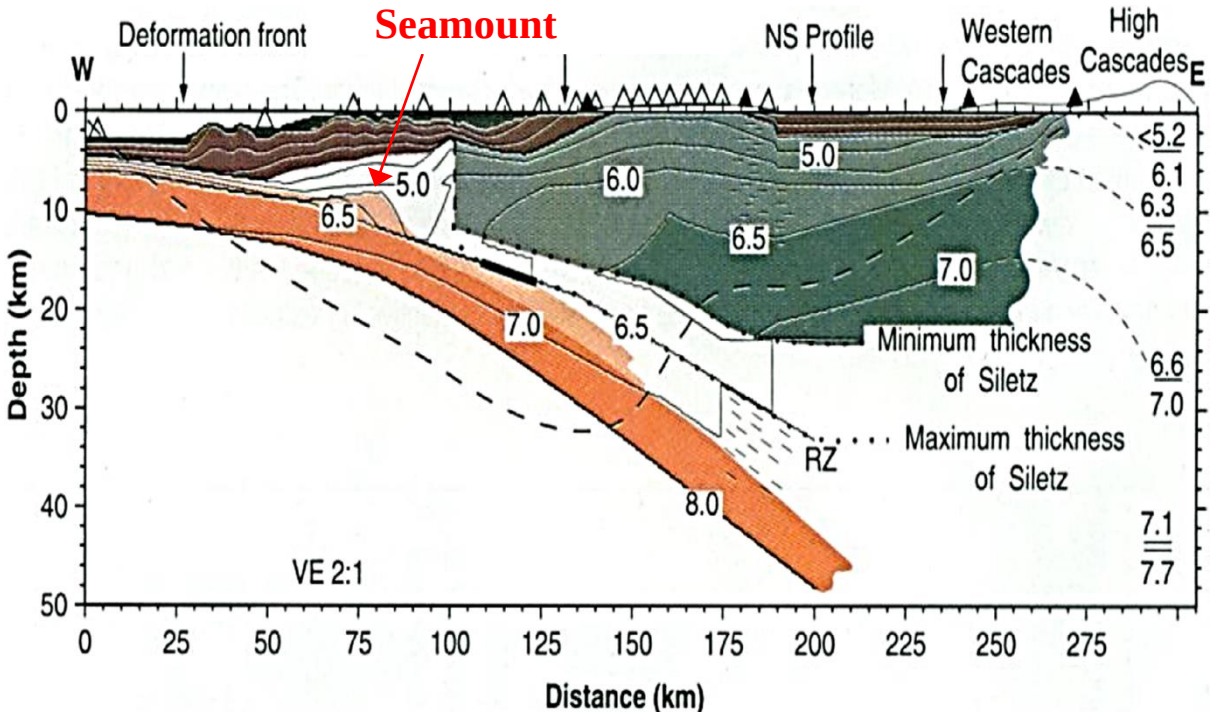

Figure 15. Result of seismic refraction experiment for the Oregon profile from Trehu et al. (1994). See location of this line in **Figure 7**.

According to Trehu et al. (1994), the interpreted stacked seamount holds up the subducting oceanic slab and causes reduced seismicity in the area around it (**Figure 2**). Other than that, the same tectonic features as in Parsons et al. (2005) can be interpreted from this velocity-structure model. These two-dimensional velocity models from Parsons et al. (2005) and Trehu et al. (1994) were used to derive geological constraints listed in **Table 5** for integrated geophysical modeling described in the next chapter.

Table 5. Thickness constraints for various tectonic features (in km) derived siesmic refraction surveys.

Location	**Thickness of oceanic crust**	**Thickness of sediments to the west of the deformation front**	**Thickness of accretionary Prism**	**Thickness of Siletz terrane**	**Thickness of the onshore sedimentary basin**
Washington transect (Parsons et al.,2005)	6	7	16	35	3
Oregon transect (Trehu et al., 1994)	6.5	7	13	35	2

Chapter 4. Integrated Two-Dimensional Geophysical Model

The integrated two-dimensional model was developed for the seismic transect through the Juan de Fuca oceanic plate shown in **Figure 16**. This model uses a free-air gravity anomaly (Sandwell et al., 2014), seismic refractions thickness constraints (**Table 5**) from the two surveys described in Chapter 3, and the central portion of the RC1501 seismic reflection survey shown in **Figure 16**. Conversion from the two-way travel time (seconds) to depths in km was done in the GM-SYS module of Geosoft software. The topography and gravity maps (**Figure 17**) were used to initiate a geophysical model in Geosoft.

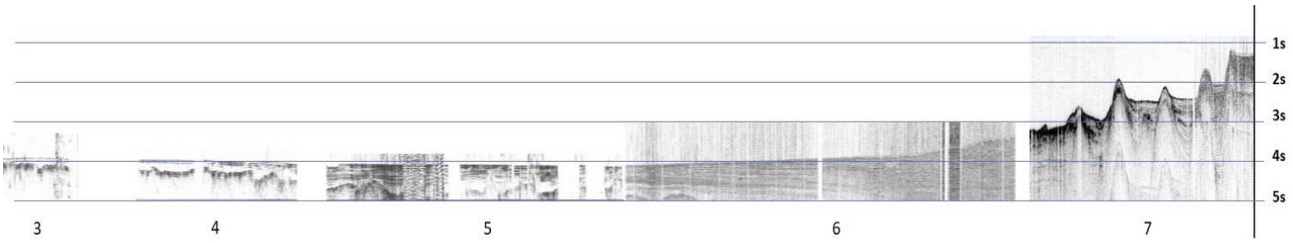

Figure 16. Two-way travel time in seconds section from RC1501 seismic reflection images across the Juan de Fuca plate. Vertical scale of the composed profile of stitched seismic images from **Figure 8b** is added and justified based on the two-way travel time instead of depth. Total profile length is 525 km.

4.1 Methodology

The following steps in Geosoft Oasis Montaj software were performed to generate the integrated geophysical model:

1. The extent of the model across the area of interest, which is the central Juan de Fuca plate, was digitized from a map shown in **Figure 17a**.
2. The stitched seismic reflection profile shown in **Figure 16** was used to constrain the shallow sedimentary features and the top of the oceanic crust to the west of the deformation front. The topography from the map shown in **Figure 17b** was extracted (marked with a bright green arrow in the 2-D model, **Figure 18**).
3. The model was divided into different layers guided by available seismic reflection and refraction data.
4. The physical property of each layer, namely density in g/cm^3, was assigned based on the expected lithology.

a.

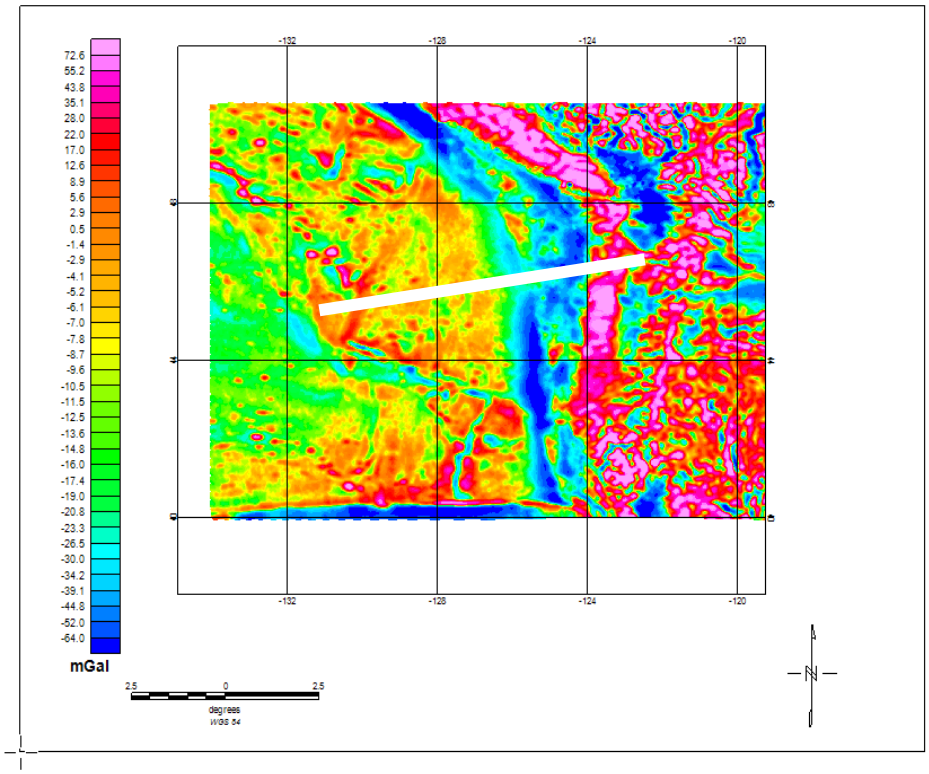

b.

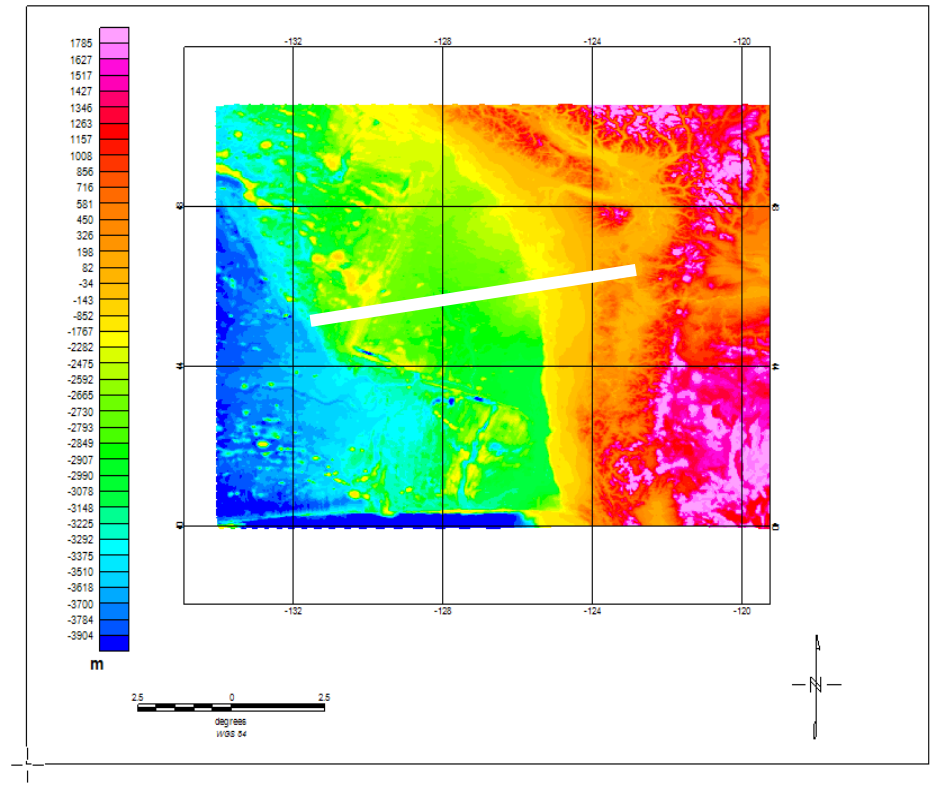

Figure 17a. Free-air gravity map from Sandwell et al. (2014). **b.** Topography map from Smith and Sandwell (1997) for the same region. The white line shows the location of the modeled profile shown in **Figures 16** and **18**.

5. The free-air gravity anomaly was then computed and compared with the observed gravity values extracted from the map shown in **Figure 17a**.
6. The model was adjusted to ensure the match between calculated and observed free-air gravity values.

4.2. Results

The integrated geophysical model is shown in **Figure 18**. The top panel is observed and computed free-air gravity anomalies. The subsurface model shown in the bottom panel of **Figure 18** consists of the following layers:

- Seawater is shown in light blue color. It is the topmost layer with a density of 1.03 g/cm^3 **(**Telford et al., 1990) and a depth of up to 3 km constrained from the bathymetry grid shown in **Figure 17b**. The alignment with the sea bottom interpreted from seismic reflections confirms the correct location of the modeled line.
- Several sedimentary layers were included based on the location within the model:
    - Oceanic sediments to the west of the deformation front (the first 190 km of the model) are right below seawater. They are shown in light green with a density of 2.2 g/cm^3 (Ashraf and Filina, 2021b). Their thickness ranges from 0 over the Juan de Fuca spreading center to a maximum of 0.5 km based on seismic reflections.
    - Folded and deformed sediments of the accretionary prism, shown in different shades of gray in **Figure 18** darkening downwards with depth, indicate increasing densities from 2.45 g/cm^3 to 2.75 g/cm^3 from top to bottom (Ashraf and Filina, 2021b). The accretionary prism starts at a distance of ~380 km from the beginning of the line and extends up to an onshore sedimentary basin on the east. It is constrained by refraction data as shown in **Table 5**. A total maximum thickness of the accretionary prism of 13 km is required to fit gravity, which is in agreement with refraction data.
    - A sedimentary basin in the continental domain is shown in bright orange in the eastmost part of the model, with a density of 2.5 g/cm^3 and a thickness of up to ~3 km from refraction data (**Table 5**). This basin extends ~100 km to the east of the accretionary wedge in northern Oregon.

- The Juan de Fuca oceanic crust and the subducting slab are shown in various shades of blue with a density varying from 2.8 g/cm^3 (light blue) in the west by the Juan de Fuca spreading ridge to 2.9 g/cm^3 (dark blue) in the subduction zone, which is consistent with the models of Ashraf and Filina (2021b). The gradual increase in density away from the spreading center relates to the cooling of oceanic crust with age. The thickness of the oceanic crust in the model is ~6.5 km that is consistent with seismic refractions (**Table 5**) and seismic reflections (**Figure 13**).
- The Siletz terrane is shown in pink in **Figure 18**. It has a density of 3.1 g/cm^3 and a thickness of 26 km in the derived model consistent with the refraction constraints listed in **Table 5**. The total extent of the Siletz terrane is ~160 km.
- The mantle is the bottommost layer (colored in red) with a density of 3.3 g/cm^3 (Telford et al., 1990). The top of the mantle, i.e., the Moho boundary, was constrained from seismic refractions data in **Figures 14** and **15** and is consistent with seismic reflections (**Figure 13**).

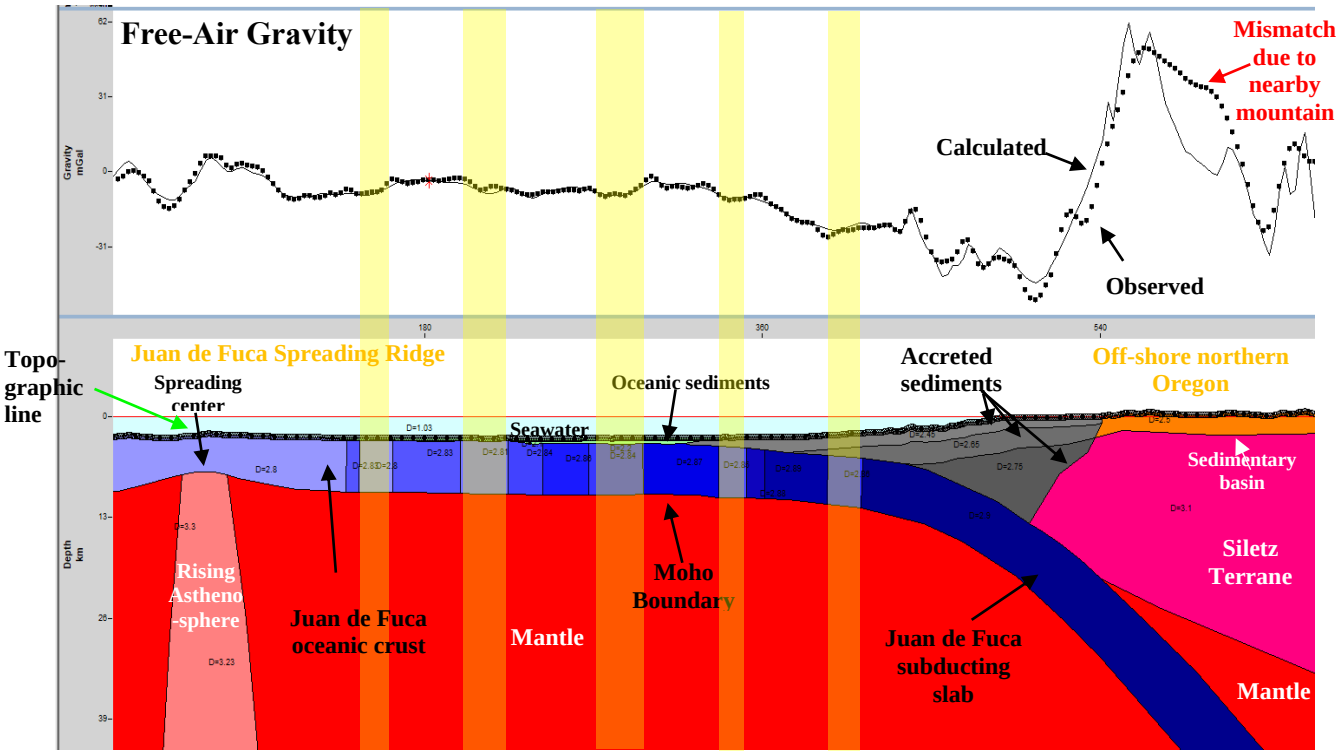

Figure 18. Geophysical gravity based subsurface model across Juan de Fuca plate through Cascadia subduction zone. The yellow highlighted blocks are the crustal low-density zones required to fit gravity data. See text for details.

- The spreading center, the westernmost part of this geophysical model, is shown in pale red, with a density of 3.23 g/cm^3. As partially molten asthenosphere rises, it causes the Juan de Fuca oceanic crust to rise and thin.

Not all features in **Figure 18** were attempted to fit. For example, there is a mismatch between the observed and calculated gravity anomaly marked with a red arrow. This mismatch results from a three-dimensional gravity effect from a mountain nearby that is not crossed by the modeled line.

The yellow highlighted blocks in Figure 18 show the regions where lower crustal density values (with respect to surrounding blocks) are required to fit the observed gravity lows. The portions of oceanic crust shown in lighter shades of blue in **Figure 18** represent lower densities. These results are consistent with the findings of Ashraf and Filina (2020, 2021a, b), who developed similar models for the Washington and Oregon transects from Han et al. (2016) and interpreted similar low-density crustal zones.

The developed geophysical model (**Figure 18**) agrees with seismic reflections, refractions, and gravity data. The fact that the model honors multiple geophysical data increases the overall confidence in the derived structures. The results of this study were presented at the annual meeting of the Nebraska Academy of Sciences in 2021 (Al Farsi et al., 2021) and the UNL Research Fair 2021 (Al Farsi, 2021).

Conclusions

The Cascadia subduction zone, located in southwestern British Colombia and the U.S. Pacific Northwest, has unevenly distributed seismic activity. The earthquakes are triggered by the subducting oceanic Juan de Fuca plate beneath the North American continental plate. This project aims to study the tectonic structures of the Juan de Fuca plate and the Cascadia subduction zone from seismic reflection and refraction data integrated with gravity anomaly. The following conclusions were drawn:

1. The database of seismic reflection and refraction data from the public domain was composed to analyze the tectonic structures of the region. Eight publicly available seismic reflection surveys acquired between 1964 and 2017 were found. Several old, low-resolution, unscaled seismic images required stitching into coherent profiles before major tectonic features could be interpreted, such as an oceanic basement, stratified sedimentary layers over the Juan de Fuca plate, seamounts, deformation front, and folds of the accretionary prism. However, the majority of seismic reflection sections did not allow the mapping of the Moho boundary and deeper tectonic features.

2. The database of published seismic refractions consists of two surveys acquired in Oregon and Washington parts of the margin, crossing the low and high seismicity zones respectively. Seismic refractions allowed the interpretation of large and deep tectonic structures of the Cascadia subduction zone, such as the base of the accretionary prism, the Siletz terrane, the continental sedimentary basin, the subducting slab, and the Moho boundary.

3. The integrated two-dimensional model across the Juan de Fuca plate was developed by combining the inputs from reflections, refractions, and gravity data. Several low-density zones in the oceanic crust are interpreted that are required to fit the observed free-air gravity anomaly. This result is consistent with the previous findings from Ashraf and Filina (2020, 2021a, b).

References

Al Farsi, K., 2021, Developing a database of seismic data over the Cascadia subduction zone. UNL Research Fair 2021. https://mediahub.unl.edu/media/16231

Al Farsi, K., Ashraf A., Al Badi, S., and Filina, I., 2021, Geological structures and crustal architecture of Juan de Fuca plate from seismic data. 141st annual meeting of Nebraska Academy of Sciences.

Ashraf, A., and Filina, I., 2020. Integrated 2D geophysical modeling over the Juan de Fuca plate, Geological Society of America Abstracts with Programs. Vol 52, No. 6 doi: 10.1130/abs/2020AM-358134

Ashraf, A., and Filina, I., 2021a, Major tectonic structures of Juan de Fuca plate from integration of seismic, gravity and magnetic data, Nebraska Academy of Sciences, Annual Meeting Abstracts 2021, p. 95

Ashraf, A., and Filina, I., 2021b, 2D integrated geophysical modeling over the Juan de Fuca plate, Geological Society of America Abstracts with Programs. Vol. 53, No. 3, 2021 doi: 10.1130/abs/2021NC-362862

Atwater, B.F., and Hemphill-haley, E., 1996, Preliminary Estimates of Recurrence Intervals for Great Earthquakes Of the Past 3500 Years at Northeastern Willapa Bay, Washington: Geology, v. 5

Canales, J., 2002, EW0207, Marine Geoscience Data System, Columbia University https://www.marinegeo.org/tools/search/DataSets.php?data_set_uids=375,3711,3763,3775,6864,27838,27839,27840,27841,27842,27843,27844,27845,27846,27847,27848,27849#datasets

Carbotte, S., and Canales, J. , 2012, MGL1211, Marine Geoscience Data System, Columbia University https://www.marine-geo.org/tools/search/Files.php?data_set_uid=19195

Carpenter, G., 1971, RC1501, Marine Geoscience Data System, Columbia University https://www.marine-geo.org/tools/search/entry.php?id=RC1501#.

DeMets, C., Gordon, G., and Argus, F., 2010, Geologically current plate motions: Geophysical Journal International, doi:10.1111/j.1365-246X.2009.04491.x.

Epp, D., 1967, RC1110, Marine Geoscience Data System, Columbia University https://www.marinegeo.org/tools/search/mapview_files.php?filespage=1&data_set_uids=3009

Flueh, Ernst R. and Fisher, Michael A., eds., 1996, FS SONNE Fahrtbericht / Cruise Report SO 108 [SO108] ORWELL - Oregon and Washington Exploration of the Lithosphere - a geophysical experiment, San Francisco - Astoria, 14.4.-23.5.1996. . GEOMAR-Report, 049 . GEOMAR Forschungszentrum für Marine Geowissenschaften, Kiel, 282 pp. DOI 10.3289/GEOMAR_REP_49_1996.

Flueh, Ernst, et al., , 1997, Scientific Teams Analyze Earthquake Hazards of the Cascadia Subduction Zone." Eos, Transactions American Geophysical Union, vol. 78, no. 15, p. 153., doi:10.1029/97eo00097.

Fray, C., 1966, RC1011, Marine Geoscience Data System, Columbia University https://www.marine-geo.org/tools/search/Files.php?data_set_uid=3001.

Goldfinger, C., Galer, S., Beeson, J., Hamilton, T., Black, B., Romsos, C., Patton, J., Nelson, C.H., Hausmann, R., and Morey, A., 2017, The importance of site selection, sediment supply, and hydrodynamics: A case study of submarine paleoseismology on the northern Cascadia margin, Washington USA: Marine Geology, doi:10.1016/j.margeo.2016.06.008.

Holbrook, S., 2012, MGL1212, National Centers for Environmental Informational, University of Wyoming https://www.ngdc.noaa.gov/ships/marcus_g_langseth/MGL1212_mb.html

Kozak, C., 2016, Seismic Testing Q&A: Pros and Cons, Newport, NC https://coastalreview.org/2016/05/14318/

Le Pichon, X., 1964, V2004, Marine Geoscience Data System, Columbia University https://www.marine-geo.org/tools/search/Files.php?data_set_uid=848.

Lillie, R., 1999.Whole earth geophysics. Oregon State University, USA.

Parsons, T., Blakely, R., Thomas M. Brocher, T. and Christensen, N., 2005. Crustal Structure of the Cascadia Fore Arc of Washington. USGS, https://pubs.usgs.gov/pp/pp1661d/

Pitman, W., 1967, RC1109, Marine Geoscience Data System, Columbia University https://www.marine-geo.org/tools/search/Files.php?data_set_uid=3008

Sandwell, D., Müller, R., Smith, W., Garcia, E., and Francis, R., 2014, New global marine gravity model from CryoSat-2 and Jason-1 reveals buried tectonic structure: Science, doi:10.1126/science.1258213.

Smith, W., and Sandwell, D., 1997, Global Sea floor topography from satellite altimetry and ship depth soundings: Science, doi:10.1126/science.277.5334.1956

Telford, W., Geldart, L., and Sheriff, R., 1990, Applied geophysics. 2nd edition: Applied geophysics. 2nd edition

Tominaga, M., 2017, RR1718, Marine Geoscience Data System, Columbia University https://www.marine-geo.org/tools/search/Files.php?data_set_uid=24504

Trehu, A., and Nabelek, J., 1994, Crustal Architecture of the Cascadia Forearc. Department of Oceanic and Atmospheric Sciences. Oregon State University.

Witter, R.C., Zhang, Y., Wang, K., Goldfinger, C., Priest, G.R., and Allan, J.C., 2012, Coseismic slip on the southern Cascadia megathrust implied by tsunami deposits in an Oregon lake and earthquake-triggered marine turbidites: Journal of Geophysical Research: Solid Earth, doi:10.1029/2012JB009404.